

Enhancement of microfluidic efficiency with nanocrystalline diamond interlayer in the ZnO-based surface acoustic wave device

H.-F. Pang · Y. Q. Fu · L. Garcia-Gancedo ·
S. Porro · J. K. Luo · F. Placido · J. I. B. Wilson ·
A. J. Flewitt · W. I. Milne · X. T. Zu

Received: 3 November 2012 / Accepted: 11 February 2013 / Published online: 3 March 2013
© Springer-Verlag Berlin Heidelberg 2013

Abstract Ultra-smooth nanocrystalline diamond (UNCD) films with high-acoustic wave velocity were introduced into ZnO-based surface acoustic wave (SAW) devices to enhance their microfluidic efficiency by reducing the acoustic energy dissipation into the silicon substrate and improving the acoustic properties of the SAW devices. Microfluidic efficiency of the ZnO-based SAW devices with and without UNCD inter layers was investigated and compared. Results showed that the pumping velocities increase with the input power and those of the ZnO/UNCD/Si devices are much larger than those of the ZnO/Si devices at the same power.

The jetting efficiency of the droplet was improved by introducing the UNCD interlayer into the ZnO/Si SAW device. Improvement in the microfluidic efficiency is mainly attributed to the diamond layer, which restrains the acoustic wave to propagate in the top layer rather than dissipating into the substrate.

Keywords Nanocrystalline diamond film · Surface acoustic wave · Pumping and jetting · Efficiency

H.-F. Pang · X. T. Zu (✉)

School of Physical Electronics, University of Electronic Science and Technology of China, Chengdu, People's Republic of China
e-mail: xtzu@uestc.edu.cn

H.-F. Pang · Y. Q. Fu (✉) · F. Placido

Thin Film Centre, Scottish Universities Physics Alliance (SUPA), University of the West of Scotland, Paisley, UK
e-mail: Richard.fu@uws.ac.uk

L. Garcia-Gancedo · A. J. Flewitt · W. I. Milne
Electrical Engineering Division, Department of Engineering,
University of Cambridge, 9 JJ Thomson Avenue,
Cambridge, UK

S. Porro · J. I. B. Wilson

School of Engineering and Physical Sciences,
Scottish Universities Physics Alliance (SUPA),
Heriot-Watt University, Edinburgh, UK

Present Address:

S. Porro
Center for Space Human Robotics,
Istituto Italiano di Tecnologia (IIT), Turin, Italy

J. K. Luo

Institute of Materials Research and Innovation (IMRI),
University of Bolton, Bolton, UK

1 Introduction

Surface acoustic wave (SAW) induced manipulation of liquid at the microscale has attracted much attention for integrated microfluidics and lab-on-chip applications (Franke and Wixforth 2008; Mark et al. 2010; Friend and Yeo 2011). Various SAW-based microfluidic functions have been widely reported, including transportation, mixing, splitting, jetting, nebulization, and concentration of particles in the droplet (Wixforth et al. 2004; Nguyen and Wu 2005; Yeo and Friend 2009; Yoon et al. 2012). Functionality of the SAW-based microfluidics device is dependent on the interdigitated transducer (IDT) electrode design and the structure and acoustic properties of the piezoelectric material substrate, which modulate the droplet actuation through the SAW/liquid interaction (Wood et al. 2009; Glass et al. 2012; Hashimoto 2011). Therefore, an optimum design of the structure (i.e., IDT pattern or multi-layer thin films) and controllable growth of high-quality piezoelectric materials are important to improve the performance of SAW-based microfluidic devices.

In order to enhance the microfluidic efficiency and reduce the input radio frequency (RF) power for manipulation of liquid using SAW devices, different approaches

have been utilized, including using modified IDT electrodes with focused or circle structures, phononic crystal structures, and special designs for the micro-channels, etc. (Tan et al. 2009; Du et al. 2009a, b; Reboud et al. 2012; Shi et al. 2009). ZnO-based SAW devices on silicon substrates possess the advantages of low cost, large-scale production, high breakdown voltage, and easy integration with silicon processing technology, which have been exploited in microfluidic applications such as liquid mixing, pumping, and jetting (Fu et al. 2010; Du et al. 2008, 2009a, b). Ultra-smooth nanocrystalline diamond (UNCD) films were also used as an interlayer between ZnO piezoelectric layer and the silicon substrate to reduce the propagation loss of the acoustic energy, and manipulation of the droplet using the ZnO/UNCD SAW device has been successfully demonstrated for microfluidic applications (Fu et al. 2012). However, it has not been shown that if the microfluidic efficiency of ZnO/UNCD/Si SAW devices is better or not compared to that of the ZnO/Si SAW structures, and the effects of the thickness of the UNCD interlayer and the ZnO film on the droplet manipulation have not been fully elucidated.

In this paper, ZnO/UNCD SAW devices with different thickness of the ZnO and UNCD films were fabricated and their microfluidic performance (pumping velocity and jetting efficiency) was compared to that of the ZnO/Si SAW devices with the same IDT design parameters.

2 Experiment details

Deposition of the UNCD coatings with various thicknesses on 4-in. (100)-oriented Si substrates was performed using a hot filament chemical vapor deposition (HFCVD) system (sp3 Diamond Technologies, model 650, Santa Clara, USA) (Porro et al. 2009). The details of the UNCD-coating deposition have been reported elsewhere (Porro et al. 2009; Fu et al. 2012). ZnO films with a thickness of about 6 μm at a deposition rate of $\sim 50 \text{ nm min}^{-1}$ were deposited on the Si substrates and UNCD-coated Si wafers using high-target utilization sputtering (HiTUS, Plasma Quest, Hampshire, UK) (Fle Witt et al. 2009; Pedrós et al. 2011; García-Gancedo et al. 2012). This technique yields high-quality films with very low stress and defect density. The details of the sputtering conditions of the ZnO films were described elsewhere (Fu et al. 2012). In order to compare the effect of the thickness of the UNCD layer on the microfluidic phenomena, the thickness of the UNCD layers is designed to be changed from 0 to 3.32 μm with the ZnO films being $\sim 6 \mu\text{m}$, which allows the observation and comparison of the microfluidic dynamics for the different acoustic properties of the ZnO-based SAW devices. The measured film thicknesses were slightly different from the designed thickness during the deposition due to the variation of the

deposition rate or duration. The cross-sectional microstructures of the ZnO/UNCD/Si films were characterized using scanning electron microscopy (SEM, S-4100, Hitachi, Tokyo, Japan). The crystallographic orientation of the ZnO films was determined using X-ray diffraction (XRD, D5000, Siemens, Munich, Germany) with Cu-K α radiation ($\lambda = 1.5406 \text{ \AA}$). The IDTs on the ZnO and ZnO/diamond layer were produced using evaporated Cr/Au thin films up to 7/50 nm thickness, and then patterned using a standard photolithography process. The resulting bi-directional IDTs were composed of 30 pairs of fingers, with a spatial periodicity of 64 μm and an aperture of 4.9 mm. The resonant frequency and amplitude of the SAW devices were measured using an RF network analyzer (HP8752A, Agilent Technologies, Santa Clara, USA).

The efficiency of the energy conversion from the electric signal to the SAW was estimated by the electromechanical coupling coefficient (k^2), which was computed using the following formula (Smith et al. 1969):

$$k^2 = \frac{\pi}{4N} \left(\frac{G}{B} \right)_{f=f_0} \quad (1)$$

where G and B are the radiation conductance and susceptance at the central frequency, respectively; N is the finger pairs of the IDT. G and B were obtained from the Smith charts of the measured reflection coefficients at the central frequency of the SAW signals.

For microfluidic testing, the surfaces of the SAW devices were then spin-coated with a CYTOP (Asahi Glass Co., Tokyo, Japan) hydrophobic layer. The contact angles were about 115° – 118° on the hydrophobic surface of the SAW device. The sinusoidal RF signal from a signal generator (Marconi 2024, Plainview, USA) was amplified using a power amplifier (Amplifier research, 75A250, Souderton, USA). The amplified signal was then sent into the input port of the RF power meter and was applied on the IDT through a 50 Ohms cable from the output port of the meter. The RF input power can be obtained before being applied onto the IDTs. Droplet movement driven by the generated SAW was captured using a high speed video camera (Photron XLR Express, Tokyo, Japan). Droplets of distilled water with volumes from 0.5 to 20 μL were obtained using a micropipette. The diameters of the droplets with volumes of 0.5, 2, 5, 10, 15, and 20 μL are about 0.85, 1.6, 2.1, 3, 3.5, and 4 mm, respectively, which are smaller than the aperture of the IDTs (4.9 mm).

3 Results and discussion

Figure 1a–d show the cross-sectional images of the ZnO/Si and ZnO/UNCD/Si microstructures used for SAW device fabrication, showing the compact columnar structures for

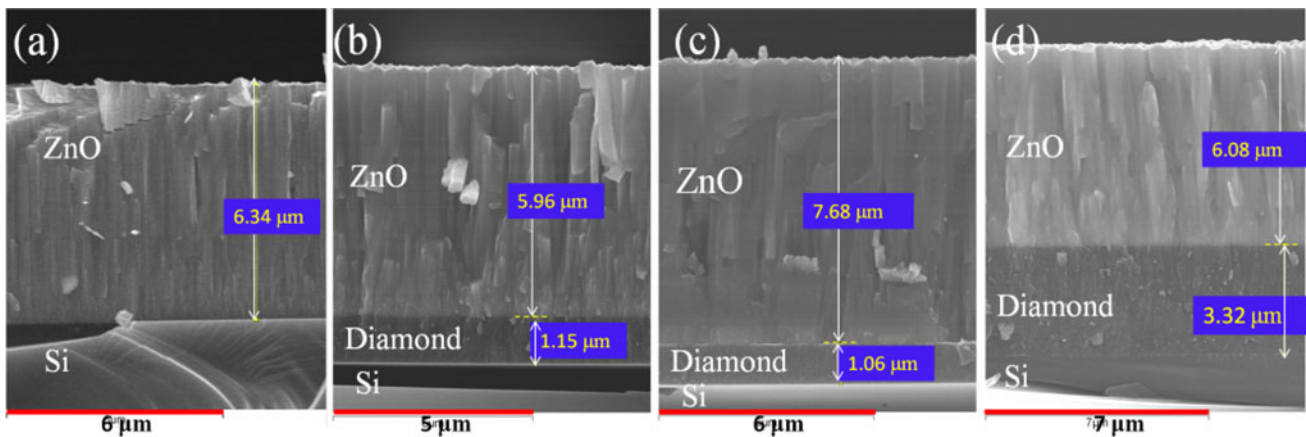


Fig. 1 Cross-section images of the ZnO/UNCD SAW devices with the thicknesses of **a** 6.34 μm ZnO film, **b** 5.96 μm ZnO and 1.15 μm UNCD films, **c** 7.68 μm ZnO and 1.06 μm UNCD films, and **d** 6.08 μm ZnO and 3.32 μm UNCD films

all films with various thicknesses of the ZnO and UNCD layers. For the XRD results shown in Fig. 2, a weak (10 $\bar{1}$ 0) peak and a dominant (0002) peak are observed, indicating the preferred *c*-axis orientation of all the highly textured ZnO films on both the silicon and the UNCD layers (diffraction peaks are indexed based on the JCPDS card No. 36-1451 (McMurdie et al. 1986)). The thicknesses of ZnO/UNCD films are 6.34/0, 5.96/1.15, 6.08/3.32, and 7.68/1.06 μm, respectively. The columnar microstructure of ZnO films does not show apparent changes on the UNCD layers of different thicknesses, because the grain size and surface roughness of the UNCD layers do not show significant differences (Porro et al. 2009).

The reflection signals of the SAW devices with different thicknesses of ZnO and UNCD films are shown in Fig. 3. Both the peaks of Rayleigh and Sezawa modes are observed in the frequency spectra, where the Sezawa mode structure is due to the triple transit effect (Fu et al. 2012; Campbell 1998; Marcelli et al. 1993). The amplitudes of the Rayleigh mode peaks are 1.19, 1.75, 1.95, and 0.92 dB for the SAW devices with ZnO/UNCD films of 6.34/0,

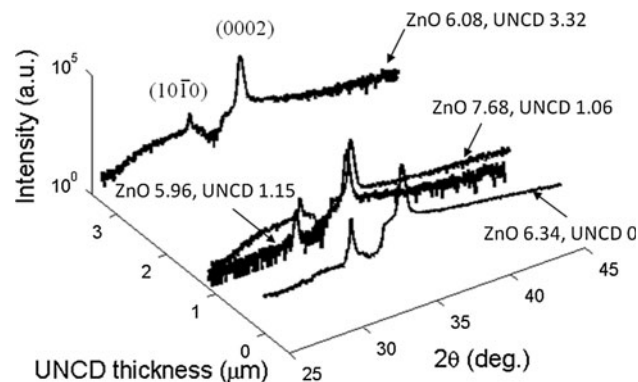


Fig. 2 X-ray diffraction patterns of ZnO films on the Si substrate and UNCD layers

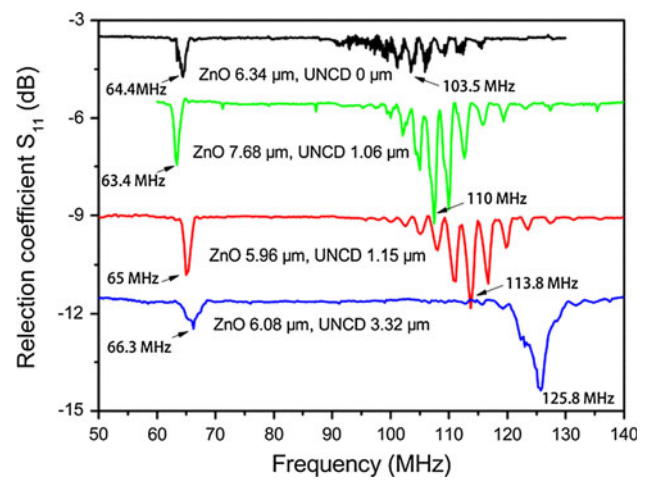


Fig. 3 Reflection coefficients (S_{11}) of the ZnO/UNCD SAW devices with different thicknesses of the UNCD and ZnO films

5.96/1.15, 7.68/1.06, and 6.08/3.32 μm, respectively (Pang et al. submitted). When the thickness of ZnO films remains ~6 μm, the frequencies of both the Rayleigh and Sezawa mode peaks increase with UNCD thickness. The introduction of the UNCD interlayer can effectively reduce the penetration depth of the Rayleigh SAW in the Si substrate, prevent energy dissipation under the UNCD layer (Nakahata et al. 2005; Mortet et al. 2008), and increase the acoustic phase velocity, thus resulting in a large value of 4243 m/s for the 6.08 μm ZnO film on the 3.32 μm UNCD layer. However, the frequencies of the Rayleigh and Sezawa mode peaks slightly decrease with increase of the ZnO film thickness for devices with an UNCD layer of ~1 μm thick.

Systematic studies on deposition of the high-quality ZnO/UNCD films and optimization of the layered structure of various thicknesses have been performed to improve the performance of the ZnO/UNCD devices (Pang et al. submitted). Figure 4 shows the coupling coefficient of the

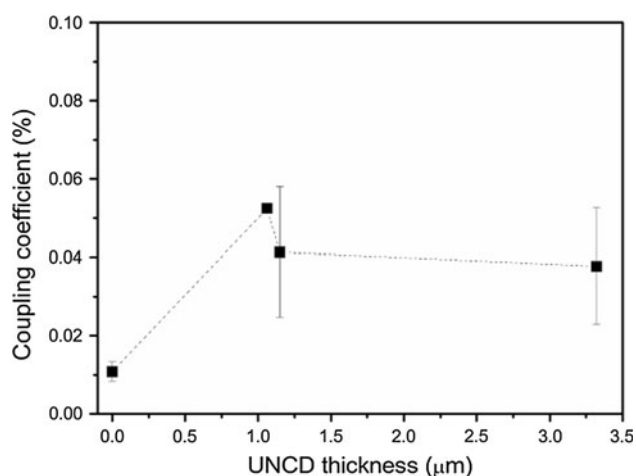


Fig. 4 Electromechanical coupling coefficients of ZnO/Si and ZnO/UNCD/Si SAW devices

ZnO/UNCD SAW devices used in this study. For the SAW device with the ZnO film deposited on Si, the calculated coupling coefficient of the Rayleigh mode SAWs is 1.08 %. Clearly, the coupling coefficient of the Rayleigh wave mode has been increased by adding a UNCD layer. When the UNCD thickness is increased from 1.06 to 3.32 μm , the coupling coefficients are varied but are still close to each other at about 4 %.

For the ZnO/UNCD/Si SAW device studied, as a function of the input power, various microfluidic phenomena, including internal streaming, pumping and jetting can be induced by the Rayleigh as well as Sezawa waves. Here, we only focus on Rayleigh wave-based microfluidics. Figure 5a shows the critical values of the input power to generate various phenomena as a function of droplet volume for the SAW devices with different thicknesses of ZnO and UNCD films. The droplet radii are much larger than the acoustic wavelength of 64 μm . The acoustic internal streaming starts to occur at an input power of ~ 20 to $\sim 1,500$ mW with the Reynolds number < 1.0 (Tan et al. 2009). The pumping of the droplet starts at a power of a few Watts. When the power is higher than ~ 18 W, a water beam due to droplet jetting can be observed with a large Reynolds number approaching $\sim 10^3$ due to the inertial stress of the droplet overcoming the surface tension (Tan et al. 2009). The critical lines indicate that the driving forces increase with input power, which is caused by the increased acoustic radiation pressure gradient in the droplet and significant dissipation near the contact line (Du et al. 2009a, b; Bonn et al. 2009; Doinikov 1996; Brunet et al. 2010). To initiate the droplet pumping or jetting, the input power applied on the same SAW device becomes much larger with an increase in the droplet volume. Results show that the ZnO/Si SAW devices require higher energy for droplet pumping and jetting than the ZnO/UNCD/Si SAW

devices for the same droplet volume. This indicates that the coupling efficiency between the acoustic wave and the liquid is enhanced by adding the UNCD interlayer into the ZnO/Si structure. Droplet pumping and jetting are generally influenced by the droplet volume, wetting properties of the surface, liquid viscosity and the property of the acoustic wave (Brunet et al. 2010; Tan et al. 2007; Guttenberg et al. 2005). When the properties of the liquid and the surface of piezoelectric film are nearly in the same conditions, the acoustic wave properties of the devices become the key factor to determine the coupling efficiency. The smooth surface of the UNCD layer (i.e., the average roughness of the UNCD layer is ~ 7 nm) can effectively reduce the propagation loss and the acoustic radiation into the Si substrate, thus resulting in the improvement of the insertion loss and amplitudes of the Rayleigh mode peaks (Nakahata et al. 2003; Le Brizoual et al. 2006). This is also beneficial to improve the electromechanical coupling coefficient. Therefore, comparing with the ZnO/Si SAW device, more acoustic energy of the ZnO/UNCD/Si SAW device can be coupled into the droplet with the same size when applied the same input power.

To investigate the effects of the droplet volume on liquid pumping, velocities of the drop motion were estimated for the ZnO/Si structures, as shown in Fig. 5b. When the power is larger than the threshold of the streaming critical line, a sessile drop deforms with asymmetric contact angles and starts to move along the propagation direction of the SAW. It can be seen that pumping velocity increases exponentially with the input power. The pumping velocities of the droplets reach maximum values before jetting occurs at a relatively high power. The pumping velocity increases with reduction of the droplet volume from 20 to 2 μL at a constant power. The pumping velocity of the 0.5 μL droplet is lower than those of the 2 μL droplets. The mass of droplet per unit contact area is estimated to be 0.97, 1.09, 1.57, 1.60, 1.84, and 1.85 mg/mm^2 for droplets with volumes of 0.5, 2, 5, 10, 15, and 20 μL , respectively. Therefore, the constant driving force in an unit contact area acting on the decreased water mass exhibits a steeper slope for the curve of the pumping velocity when the droplet volume is decreased to 2 μL . The nonlinear influence of the input power on the pumping velocity of the droplet agrees with the reports that the drop velocity increases with the enhancement of the acoustic amplitude using a LiNbO_3 SAW device (Brunet et al. 2010).

The microfluidic performance of the ZnO/UNCD/Si SAW devices was evaluated and compared with those of the ZnO/Si SAW devices. The pumping velocities of the 5 and 20 μL droplets were calculated and the curves are fitted in Fig. 6a and b, respectively. For the 5 μL droplet, the pumping velocity of the droplet for the SAW device

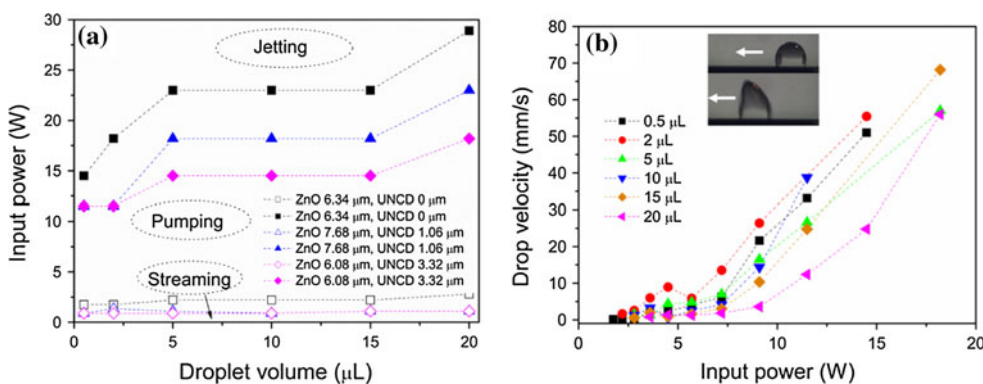
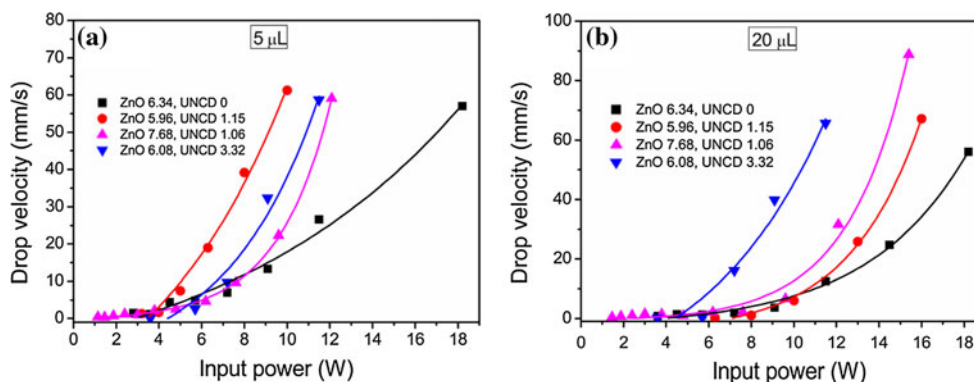


Fig. 5 **a** Results of the critical input power as functions of droplet volumes, and comparisons of the *critical lines* among jetting, pumping and streaming phenomena for the different ZnO/UNCD SAW devices, **b** pumping velocity of the droplets with different

volumes as functions of the input power for the SAW device with a 6.34-μm ZnO film on Si substrate, the *inset* shows the pumping of the 5 μL droplet driven by the Rayleigh SAW at an input power of 11.5 W and the *white arrow* shows the direction of motion

Fig. 6 Pumping velocities of the droplet with a volume of **a** 5 μL and **b** 20 μL as a function of the input power for the SAW devices with different thicknesses of the ZnO and UNCD films; the *solid lines* represent the best exponential fit



with a 5.96 μm thick ZnO film and ~1-μm thick UNCD films shows the highest value for all the SAW devices as presented in Fig. 6a. The pumping velocities for all the ZnO/UNCD/Si SAW devices show steeper slopes than that for the ZnO SAW device due to the significant reduction of the acoustic energy dissipation from the UNCD interlayer. When the droplet volume is increased to 20 μL, the upward slopes of the data become much steeper when the thickness of the UNCD interlayer is increased from 0 to 3.32 μm as shown in Fig. 6b. The SAW device with a 7.68 μm ZnO film on the ~1-μm UNCD layer results in a steeper upward-slope for the pumping velocity than that of the device with a 5.96 μm ZnO and ~1-μm UNCD films, because the former has a larger coupling coefficient and amplitude of the Rayleigh mode peak (Pang et al. submitted). This shows that the transport efficiency of the droplet can be improved by the UNCD interlayer for the ZnO-based SAW device.

Based on the analysis of the curve fitting, the empirical relation between the pumping velocity, V_{pumping} , and input power, P , can be obtained by the following equation

$$V_{\text{pumping}} = ae^{P/\beta} + b \tag{2}$$

where a , b , and β are constants, which are mainly dependent on the droplet volume, wetting properties of the surface, the liquid viscosity, and the electromechanical coupling property of the acoustic wave. Of course, the pumping velocity is also strongly correlated to the temperature of the surface and droplet. For the ZnO/UNCD/Si SAW device with a 5.96-μm thick ZnO layer and 1.15-μm thick UNCD films, the temperature inside a droplet of 20 μL was measured using thermo-camera and found to increase from 25 to 50 °C with a driving power of 11.5 W after 2 min. In general, the pumping only took about up to a few seconds. If we consider the heating effect of the SAW devices with the temperature changes from 25 to 50 °C, the viscosity and surface tension of the water drop varied from 0.890×10^{-3} to 0.547×10^{-3} Pa s and from 71.99×10^{-3} to 67.94×10^{-3} N/m, respectively, estimated from refs (Vargaftik et al. 1983; Kestin et al. 1978). However, this thermal effect will not significantly influence the pumping efficient. When the electromechanical coupling coefficient of the ZnO/UNCD/Si SAW devices increases from 1.08 to 5.2 %, the temperature differences among the surfaces of the devices were about ~2 °C at an applied power of 7.2 W and about ~6 °C at an applied

power of 15.2 W. A larger electromechanical coupling coefficient of the SAW device results in a stronger conversion of the electric energy to the SAW and more coupled acoustic energy in liquid, which can be improved by the UNCD interlayer between the ZnO film and Si substrate, as well as improvement of the piezoelectric properties of ZnO film.

The driving forces for the droplet pumping are related to the balance between the acoustic pressure gradient and the viscous energy dissipation near the contact-line where the three phases of solid/liquid/gas meet (Du et al. 2009a, b; Mortet et al. 2008; Doinikov 1996). The droplet deformation induced by the driving forces can be expressed by the capillary number, Ca , which is a relative effect of the viscous forces on surface tension, defined by the following equation (Brunet et al. 2010; Squires and Quake 2005)

$$Ca = \frac{\eta V}{\gamma} \quad (3)$$

where η , V , and γ are the viscosity, velocity, and surface tension of the water drop, respectively. Surface tension forces are generally dominant and the droplet remains spherically shaped at low capillary numbers. For large capillary number (i.e., $Ca > 0.1$), the initial spherical droplet is dominated by viscous forces and deforms into an ellipsoidal shape and eventually breaks into smaller droplets (Mulligan and Rothstein 2011). For small acoustic capillary numbers ($Ca \leq 0.001$), the capillary stress dominates over the acoustic force, and when the value is >0.01 , a capillary wave appears at the liquid/air interface (Qi et al. 2008). Figure 7 shows the capillary numbers Ca versus droplet volume for different ZnO/UNCD/Si SAW devices at the same input power of 7.2 W. A maximum value of the capillary number Ca was obtained for a droplet with volume of 2 μL , showing the most significant deformation of the droplet. All the Ca values are much lower than 0.1 which indicates that no breakup of the droplet occurs during the pumping process (Mulligan and Rothstein 2011; Anna and Mayer 2006). Moreover, the capillary number of the droplet for the ZnO SAW device is much less than those of the ZnO/UNCD SAW devices, probably due to the relatively small coupling coefficient of the ZnO SAW device and the dissipation of the acoustic energy into the Si substrate (Pang et al. submitted). When the droplet size decreases from 20 to 0.5 μL , the capillary number for ZnO/UNCD SAW devices is expected to be largest at 0.5 μL under the same input power; however, it exhibits anomaly which also appears for the droplet pumping in Fig. 5b. The possible reason is from the roughness and surface microstructure of the CYTOP polymer film, which causes a decrease of the contact angle at 0.5 μL (Tsai et al. 2010; Jopp et al. 2004).

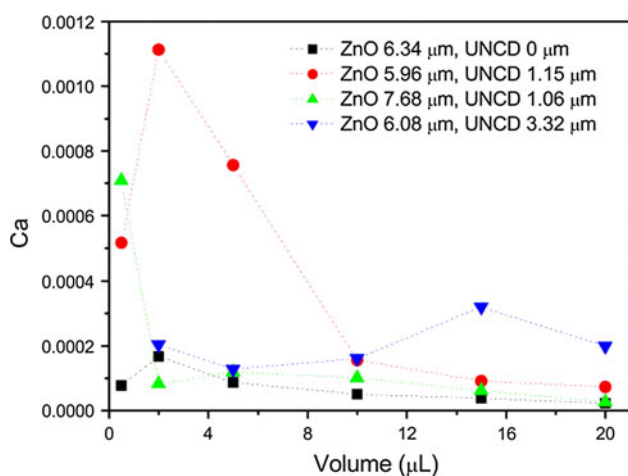


Fig. 7 Capillary numbers versus droplet volume for different ZnO/UNCD SAW devices at the same input power of 7.2 W

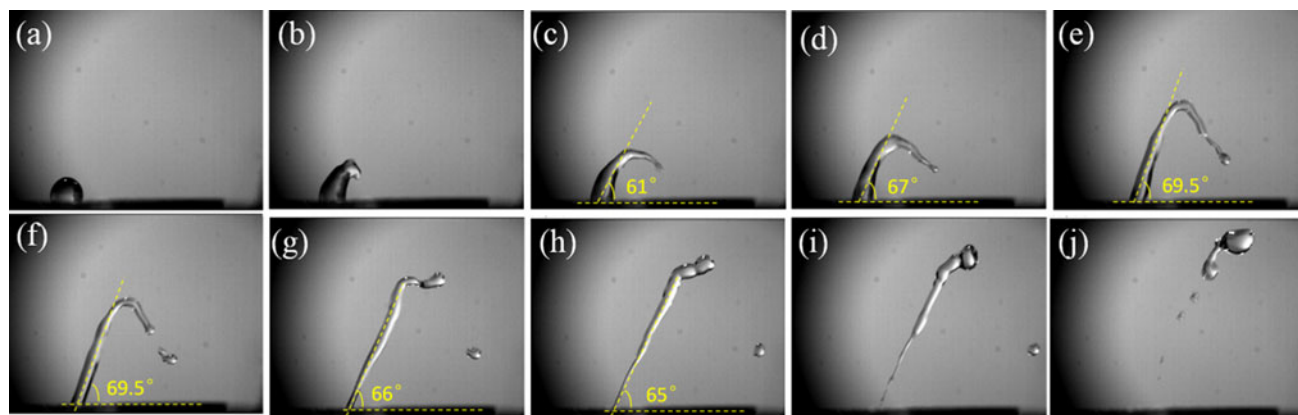


Fig. 8 High-speed jetting images of the 5 μL droplet driven by the Rayleigh mode SAW (from left to right) at a power of 36.5 W **a** 0 s, **b** 3.2 ms, **c** 9.8 ms, **d** 12.4 ms, **e** 13 ms, **f** 16 ms, **g** 17 ms, **h** 18 ms,

i 19 ms, **j** 21 ms using the ZnO/UNCD/Si SAW device with 6.08 μm ZnO and 3.32 μm UNCD films

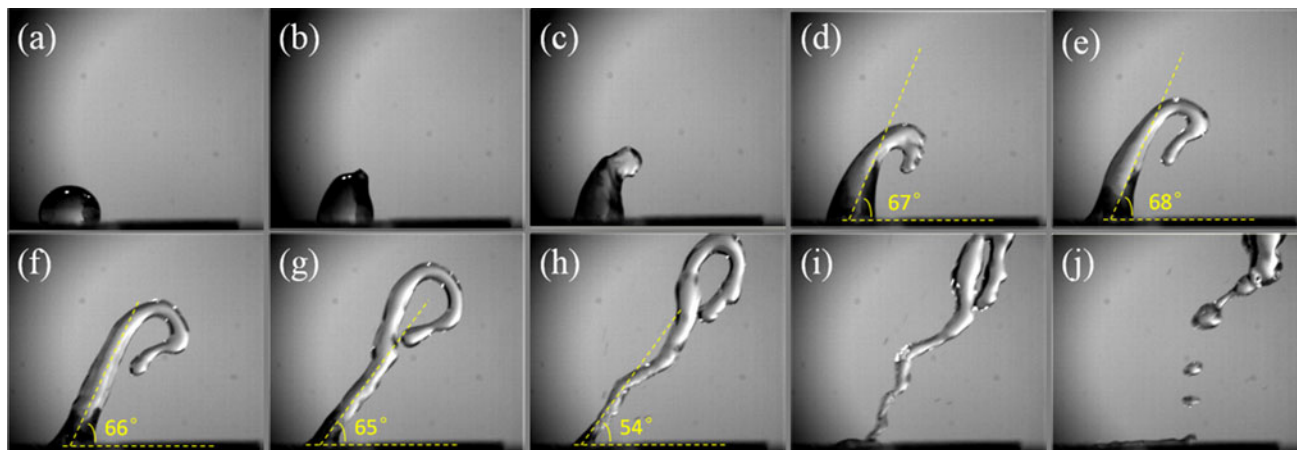


Fig. 9 High-speed jetting images of the 20 µL droplet driven by the Rayleigh mode SAW (from left to right) at a power of 36.5 W **a** 0 s, **b** 5.2 ms, **c** 9.6 ms, **d** 11 ms, **e** 13.4 ms, **f** 14.6 ms, **g** 17.4 ms,

h 19.6 ms, **i** 21.4 ms, **j** 23.6 ms using the ZnO/UNCD/Si SAW device with 6.08 µm ZnO and 3.32 µm UNCD films

In this study, the pumping velocities of the droplet for the ZnO SAW and ZnO/UNCD/Si SAW devices are found to be 0.1–90 mm/s, which is within the reported values for the ZnO-based or LiNbO₃ SAW devices (Yeo and Friend 2009; Du et al. 2009a, b; Renaudin et al. 2006). Generally the reduction of the input power in order to reach the same velocity can effectively improve the droplet transportation efficiency and decrease the energy consumption. This is dependent on the enhanced performance of the SAW device and is often realized by introducing high acoustic velocity materials such as diamond, sapphire, and diamond-like carbon (Luo et al. 2007; Mitsuyu et al. 1980; Tang et al. 2003). The results from this study confirm that adding the UNCD layer can enhance the droplet pumping efficiency for various ZnO-based SAW devices as shown in Fig. 6. The microfluidic efficiency is enhanced for the same droplet size mainly due to the increase of the driving force, which is influenced by the coupling efficiency between the SAWs and the fluids as well as the retention of the SAWs near the surface of the devices. The above two factors are related to each other. The high-quality ZnO films deposited using the advanced HiTUS technique allow the good excitation of the SAW due to the high piezoelectricity. The UNCD interlayer with a low surface roughness can further reduce the dissipation of the acoustic energy into the Si substrate and reduce penetration depth of the Rayleigh wave into the Si substrate, resulting in a stronger Rayleigh mode peak and the reduction of the propagation loss (Nakahata et al. 2005; Mortet et al. 2008). The electromechanical coefficient is also increased by the UNCD-modified ZnO/Si structure as shown in Fig. 4 (Mortet et al. 2008; Nakahata et al. 2003). Therefore, a larger driving force is obtained by the increased amplitude of the SAW in the acoustic–liquid interaction.

Significant droplet jetting using the ZnO/UNCD/Si SAW device has been realized at relatively high powers. Jetting images of a 5 µL sessile droplet are captured at the high rate of 1,000 frames per second as shown in Fig. 8 using a ZnO/UNCD/Si SAW device with 6.08-µm thick ZnO and 3.32-µm thick UNCD films. The sessile droplet was initially deformed into a short beam with a column shape (Fig. 8b) when the Rayleigh SAW refracts into the water droplet at a Rayleigh angle θ_R of 20.95° (Fu et al. 2012). With acoustic energy continuously coupled into the droplet, the water beam or column is changed into an inverted “V” shape as shown in Fig. 8c–e. The measured jetting angles are from 61° to 69.5°, and the refracted angle

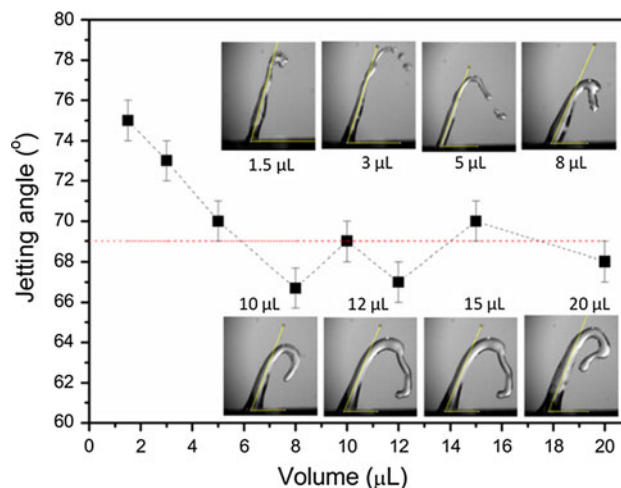
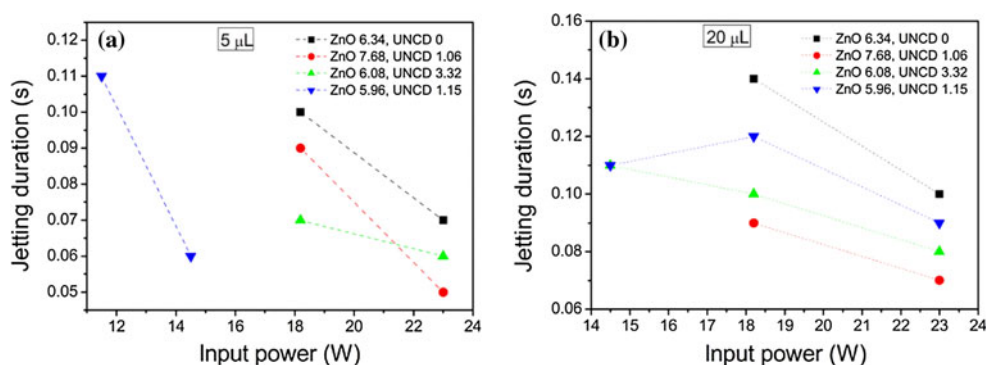


Fig. 10 Maximum jetting angle of the droplet as a function of the volume at an input power of 36.5 W performed using the ZnO/UNCD/Si SAW device with 6.08-µm ZnO and 3.32-µm UNCD films, the inset shows the beam shape of the water droplet with a volume from 1.5 to 20 µL

Fig. 11 Jetting duration of the droplet with a volume of **a** 5 μL and **b** 20 μL as a function of input power for the SAW devices with different thicknesses of the ZnO and UNCD films



of the SAW into the liquid is close to the Rayleigh angle. A droplet of $\sim\text{pL}$ is broken up at the end of the bent column (Fig. 8f) and the jetting angle decreased from 69.5° to 65° as shown in Fig. 8g and h. The elongated beam was continuously ejected until the entire droplet was consumed. At the end of the jetting process, a long filament was formed and collapsed into smaller droplets due to the Rayleigh-Plateau instability (Fig. 8i, j) (Rayleigh 1879; Eggers and Villermaux 2008). Some smaller droplets with volumes of $\sim\text{pL}$ were also observed which were ejected from the residual liquid of the droplet on the surface of the SAW device.

The jetting phenomena of a 20 μL droplet are shown in Fig. 9 using the same input power applied on the same ZnO/UNCD/Si SAW device with 6.08- μm ZnO and 3.32- μm UNCD films. The variation of the jetting angle with time is also observed in the range 54° – 68° and the minimum refracted angle of 22° is near to the Rayleigh angle. The capillary instability leading to breaking-up of smaller droplets also occurs when the whole liquid beam is ejected out of the surface (Fig. 9i, j). Clearly the maximum jetting angle is also dependent on the droplet volume in the range 1.5–8 μL during the jetting duration as shown in Fig. 10. The maximum jetting angle oscillates around 69° for droplets larger than 8 μL , corresponding to a refracted angle of 21° . The shape of the liquid beam changes from an approximately straight column, through an inverted “V” shape to a shape of swan’s curved neck with an increase in the volume from 1.5 to 20 μL . The shape change is possibly caused by the strong propagating loss of the acoustic radiation at the end of the extremely bent liquid beam when the volume is relatively large.

The jetting efficiency of a droplet with the same volume was estimated comparing the jetting durations at the same input power for all the ZnO-based SAW devices. Figure 11 shows the jetting durations of the droplets with different volumes versus the input power. The jetting durations rapidly decrease with increase of the input power for the 5 μL droplet. This indicates that the large acoustic energy and momentum coupled into the same droplet results in a

strong inertial stress to rapidly overcome the surface tension of the drop and decrease the jetting time of the cylindrical liquid column from the parent droplet (Tan et al. 2007). The jetting duration is also found to significantly decrease with increase in thickness of the UNCD film at the same power (Fig. 11b). Compared with those of the ZnO SAW devices, the jetting durations of the droplet for the ZnO/UNCD SAW devices are obviously much shorter as shown in Fig. 11b. Results clearly indicate that the jetting efficiency of the droplet can be improved by addition of an UNCD interlayer in ZnO-based SAW devices, which is promising for pumping and manipulating the liquid sample in the lab-on-chip and the SAW based liquid processing micro-systems (Olsson and El-Kady 2009; Franke et al. 2009).

4 Conclusions

In this study, UNCD films with high acoustic velocity were applied to enhance the microfluidic efficiency through reducing the acoustic energy dissipation into the substrate and improving the acoustic properties of SAW devices. The microfluidic efficiency of the ZnO-based SAW devices was investigated using the detected Rayleigh waves. Droplet pumping and jetting with different volumes were compared for the SAW devices with and without UNCD inter layers. Results show that the pumping velocities increase exponentially with the input power and those of the ZnO/UNCD/Si devices are much larger than those of the ZnO/Si devices at the same power. The jetting efficiency of the droplet was improved by introducing a UNCD interlayer compared to the ZnO/Si SAW device. The large thickness of the UNCD interlayer effectively helped to couple more acoustic energy into the liquid and resulted in a much more efficient droplet manipulation.

Acknowledgments The authors acknowledge support from the Fundamental Research Funds for the Central Universities (ZYGX 2009J046 and ZYGX2009X007), and the Sichuan Young Scientists Foundation (2010JQ0006), the Royal Society-Research Grant

(RG090609), Carnegie Trust Funding, Royal Society of Edinburgh, Royal Academy of Engineering-Research Exchanges with China and India Awards. L. García-Gancedo, A.J. Flewitt and W.I. Milne acknowledge the financial support of the EPSRC, through grants number EP/F063865/1 and EP/F06294X/1. L. García-Gancedo also acknowledges the support from the National Natural Science Foundation of China (NSFC) through grant number 61150110485.

References

- Anna SL, Mayer HC (2006) Microscale tipstreaming in a microfluidic flow focusing device. *Phys Fluids* 18:121512
- Bonn D, Eggers J, Indekeu J et al (2009) Wetting and spreading. *Rev Mod Phys* 81(2):739–805
- Brunet P, Baudion M, Bou Matar O et al (2010) Droplet displacements and oscillations induced by ultrasonic surface acoustic waves: a quantitative study. *Phys Rev E* 81:036315
- Campbell CK (1998) Surface acoustic wave devices for mobile and wireless communications. Academic Press, New York
- Doinikov AA (1996) Theory of acoustic radiation pressure for actual fluids. *Phys Rev E* 54(6):6297–6303
- Du XY, Fu YQ, Tan SC et al (2008) ZnO film thickness effect on surface acoustic wave modes and acoustic streaming. *Appl Phys Lett* 93:094105
- Du XY, Fu YQ, Luo JK et al (2009a) Microfluidic pumps employing surface acoustic waves generated in ZnO thin films. *J Appl Phys* 105:024508
- Du XY, Swanwick ME, Fu YQ et al (2009b) Surface acoustic wave induced streaming and pumping in 128° Y-cut LiNbO₃ for microfluidic applications. *J Micromech Microeng* 19:035016
- Eggers J, Villermaux E (2008) Physics of liquid jets. *Rep Prog Phys* 71:03660
- Flewitt AJ, Dutton JD, Beecher P et al (2009) Stability of thin film transistors incorporating a zinc oxide or indium zinc oxide channel deposited by a high rate sputtering process. *Semicond Sci Technol* 24(8):085002
- Franke TA, Wixforth A (2008) Microfluidics for miniaturized laboratories on a chip. *Chem Phys Chem* 9:2140–2156
- Franke T, Abate AR, Weitz DA et al (2009) Surface acoustic wave (SAW) directed droplet flow in microfluidics for PDMS devices. *Lab Chip* 9:2625–2627
- Friend JR, Yeo LY (2011) Microscale acoustofluidics: microfluidics driven via acoustics and ultrasonics. *Rev Mod Phys* 83(2):647–704
- Fu YQ, Luo JK, Du XY et al (2010) Recent developments on ZnO films for acoustic wave based bio-sensing and microfluidic applications: a review. *Sens Actuators B* 143:606–619
- Fu YQ, García-Gancedo L, Pang HF et al (2012) Microfluidics based on ZnO/nanocrystalline diamond surface acoustic wave devices. *Biomicrofluidics* 6:024105
- García-Gancedo L, Pedrós J, Zhu Z et al (2012) Room-temperature remote-plasma sputtering of c-axis oriented zinc oxide thin films. *J Appl Phys* 112:014907
- Glass NR, Shilton RJ, Chan PPY et al (2012) Miniaturized Lab-on-a-Disc (miniLOAD). *Small* 8:1881–1888
- Guttenberg Z, Müller H, Habermüller H et al (2005) Planar chip device for PCR and hybridization with surface acoustic wave pump. *Lab Chip* 5:308–317
- Hashimoto K (2011) Demands of highly piezoelectric materials for radio frequency acoustic wave devices. *Phys Stat Sol (a)* 208(5):1084–1092
- Jopp J, Grull H, Yerushalmi-Rozen R (2004) Wetting behavior of water droplets on hydrophobic microtextures of comparable size. *Langmuir* 20(23):10015–10019
- Kestin J, Sokolov M, Wakeham WA (1978) Viscosity of liquid water in the range –8–150 °C. *J Phys Chem Ref Data* 7(3):941–948
- Le Brizoul L, Sarry F, Moreira F et al (2006) FEM modelling of surface acoustic wave in diamond layered structure. *Phys Stat Sol (a)* 203(12):3179–3184
- Luo JK, Fu YQ, Le HR et al (2007) Diamond and diamond-like carbon MEMS. *J Micromech Microeng* 17:S147–S163
- Marcelli R, Rossi M, De Gasperi P (1993) End reflections and triple transit contribution to the band shape of magnetostatic volume wave delay lines. *J Appl Phys* 73:3082–3086
- Mark D, Haeblerle S, Roth G et al (2010) Microfluidic lab-on-a-chip platforms: requirements, characteristics and applications. *Chem Soc Rev* 39:1153–1182
- McMurdie H, Morris M, Evans E et al (1986) Standard X-Ray diffraction powder patterns from the JCPDS Research Association. *Powder Diffr* 1(2):76–77
- Mitsuyu T, Ono S, Wasa K (1980) Structures and SAW properties of rf-sputtered single-crystal films of ZnO on sapphire. *J Appl Phys* 51:2464–2470
- Mortet V, Williams OA, Haenen K (2008) Diamond: a material for acoustic devices. *Phys Stat Sol (a)* 205(5):1009–1020
- Mulligan MK, Rothstein JP (2011) The effect of confinement-induced shear on drop deformation and breakup in microfluidic extensional flows. *Phys Fluids* 23:022004
- Nakahata H, Fujii S, Higaki K et al (2003) Diamond-based surface acoustic wave devices. *Semicond Sci Technol* 18:S96–S104
- Nakahata H, Hachigo A, Higaki K et al (2005) Effect of crystalline quality of diamond film to the propagation loss of surface acoustic wave devices. *IEEE Trans Ultrason Ferroelectr Freq Control* 52(10):1817–1822
- Nguyen N-T, Wu Z (2005) Micromixers—a review. *J Micromech Microeng* 15:R1–R16
- Olsson RH III, El-Kady I (2009) Microfabricated phononic crystal devices and applications. *Meas Sci Technol* 20:012002
- Pang HF, García-Gancedo L, Fu YQ, Porro S, Gu YW, Luo JK, Zu XT, Placido F, Wilson JIB, Flewitt AJ, Milne WI Surface acoustic wave devices based on ZnO/ultra-nanocrystalline diamond structures. *Phys Stat Sol (a)* (submitted)
- Pedrós J, García-Gancedo L, Ford CJB et al (2011) Guided propagation of surface acoustic waves and piezoelectric field enhancement in ZnO/GaAs systems. *J Appl Phys* 110:103501
- Porro S, De Temmerman G, Ligo S et al (2009) Nanocrystalline diamond coating of fusion plasma facing components. *Diam Relat Mater* 18(5–8):740–744
- Qi A, Yeo LY, Friend JR (2008) Interfacial destabilization and atomization driven by surface acoustic waves. *Phys Fluids* 20:074103
- Rayleigh L (1879) On the capillary phenomena of jets. *Proc Roy Soc Lond* 29:71–97
- Reboud J, Bourquin Y, Wilson R et al (2012) Shaping acoustic fields as a toolset for microfluidic manipulations in diagnostic technologies. *PNAS* 109(38):15162–15167
- Renaudin A, Tabourier P, Zhang V et al (2006) SAW nanopump for handling droplets in view of biological applications. *Sens Actuators B* 113(1):389–397
- Shi J, Huang H, Stratton Z et al (2009) Continuous particle separation in a microfluidic channel via standing surface acoustic waves (SSAW). *Lab Chip* 9:3354–3359
- Smith WR, Gerard HM, Collins JH et al (1969) Analysis of interdigital surface wave transducers by use of equivalent circuit model. *IEEE Trans Microwave Theory Tech* MTT-17(11):856–864
- Squires TM, Quake SR (2005) Microfluidics: fluid physics at the nanoliter scale. *Rev Mod Phys* 77(3):977–1026
- Tan MK, Friend JR, Yeo LY (2007) Microparticle collection and concentration via a miniature surface acoustic wave device. *Lab Chip* 7(5):618–625

- Tan MK, Friend JR, Yeo LY (2009) Interfacial jetting phenomena induced by focused surface vibrations. *Phys Rev Lett* 103:024501
- Tang I-T, Wang YC, Hwang WC et al (2003) Investigation of piezoelectric ZnO film deposited on diamond like carbon coated onto Si substrate under different sputtering conditions. *J Cryst Growth* 252(1–3):190–198
- Tsai P, Lammertink RGH, Wessling M et al (2010) Evaporation-triggered wetting transition for water droplets upon hydrophobic microstructures. *Phys Rev Lett* 104(11):116102
- Vargaftik NB, Volkov BN, Voikak LD (1983) International table of the surface tension of water. *J Phys Chem Ref Data* 12(3):817–820
- Wixforth A, Strobl C, Gauer C et al (2004) Acoustic manipulation of small droplets. *Anal Bioanal Chem* 379:982–991
- Wood CD, Cunningham JE, O’Rourke R et al (2009) Formation and manipulation of two-dimensional arrays of micron-scale particles in microfluidic systems by surface acoustic waves. *Appl Phys Lett* 94:054101
- Yeo L, Friend JR (2009) Ultrafast microfluidics using surface acoustic waves. *Biomicrofluidics* 3(1):012002
- Yoon SH, Huang Y, Edgar JS et al (2012) Surface acoustic wave nebulization facilitating lipid mass spectrometric analysis. *Anal Chem* 84:6530–6537